SC-R-65-899

Sandia Corporation

REPRINT

PIEZOELECTRIC CURRENT FROM SHOCK-LOADED QUARTZ — A SUBMICROSECOND STRESS GAUGE

by

R. A. Graham, F. W. Neilson,

and

W. B. Benedick

AUGUST 1965

Issued by
Sandia Corporation,
a prime contractor to the
United States Atomic Energy Commission

Reprinted from JOURNAL OF APPLIED PHYSICS, Vol. 36, No. 5, 1775–1783, May 1965

Piezoelectric Current from Shock-Loaded Quartz— A Submicrosecond Stress Gauge

R. A. GRAHAM, F. W. NEILSON, AND W. B. BENEDICK*
Sandia Laboratory, Albuquerque, New Mexico
(Received 10 August 1964)

Current from X-cut quartz disks may be used to detect stress–time profiles induced by shock loading. The current amplitude and its time dependence are functions of the dielectric, piezoelectric, and mechanical properties of quartz under shock-loading conditions. The results of an extensive experimental study of the current from shock-loaded quartz disks are reported for shock stress up to 50 kbar. The experiment is performed by impacting precisely aligned X-cut quartz disks upon each other at various measured velocities and observing the current in one of the disks during the first wave transit. Within the low signal range, the piezoelectric stress constant e_{11} is found to be 0.174 C-m^{-2}. The coefficient relating current jump to stress jump in one-dimensional strain is found to be 2.04×10^{-8} C-cm^{-2}-kbar^{-1} up to 6 kbar and 2.15×10^{-8} C-cm^{-2}-kbar^{-1} from 9 to 18 kbar. The wave velocity was determined to be constant to 25 kbar. The observed current waveform could be fully interpreted in terms of rate-independent properties. Determinations of distortions to the current from apparently minor deviations from one-dimensional conditions were also made.

INTRODUCTION

SEVERAL recent articles[1–3] have demonstrated that current from X-cut quartz disks may be used for continuous observation on a submicrosecond time scale of stress–time profiles produced by shock loading. This quartz gauge is useful for stress up to 10's of kilobars with time resolution limited only by the planarity of the wave and the frequency response of the system used to record the gauge signal. The superior time resolution and sensitivity of the quartz gauge have enabled observations of mechanical behavior of solids under shock loading that are not possible with slower time-resolution techniques. A typical stress–time profile such as may be recorded on a routine basis is shown in Fig. 1.

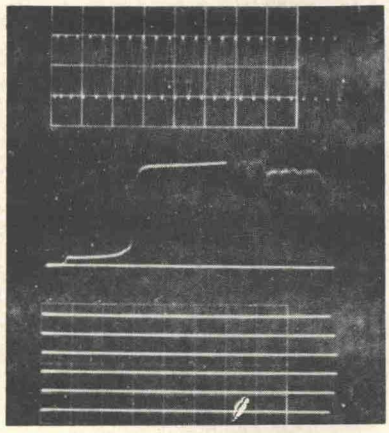

FIG. 1. Typical stress–time record obtained by recording the current from an X-cut quartz disk in direct contact with a shock-loaded specimen of a nickel–iron alloy. Time increases from left to right. 10-Mc/sec timing wave. Stress amplitude for the second wave is 45 kbar in the alloy sample.

The use of a quartz disk as a gauge requires the verification of basic assumptions concerning the physical properties of quartz, as well as quantitative clarification of the effects of minor deviations from the idealized conditions. It is the object of this paper to describe in quantitative detail the current–time characteristics of shock-loaded quartz disks in various configurations. Considerable error in interpretation of the current–time history is possible if the current distortions as outlined here are not considered.

PIEZOELECTRIC CURRENT ANALYSIS

The superior time resolution of the quartz gauge is a consequence of the observation of the short-circuit piezoelectric current during the time that the stress wave propagates along the thickness of the gauge. This is in contrast to the more conventional technique[4,5] of observing the piezoelectric charge on a time scale which is long compared to stress wave transit time in the gauge. In the latter case, the entire disk is assumed to be uniformly stressed at a given instant of time in a quasistatic state, and the piezoelectric charge is proportional to the stress in the disk. For the gauge considered in the present paper the piezoelectric current is proportional to the difference in stress at the electrodes of the disk. To understand the operation of the gauge, we must consider the piezoelectric current produced during the propagation of a stress wave along the x axis of a quartz disk.

Consider an X-cut quartz disk to one face of which a rapidly changing impulsive load is applied. Assume: (a) that the stressed region of the disk is in a state of one-dimensional strain, (b) that the electric fields produced by the piezoelectric effect are one-dimensional, (c) that the stress is instantaneously applied to the

* This work was supported by the United States Atomic Energy Commission. Reproduction in whole or in part is permitted for any purpose of the U. S. Government.
[1] O. E. Jones, F. W. Neilson, and W. B. Benedick, J. Appl. Phys. **33**, 3224 (1962).
[2] W. J. Halpin, O. E. Jones, and R. A. Graham in "Symposium on Dynamic Behavior of Materials," ASTM Special Technical Publication No. 336, American Society for Testing and Materials (1963).
[3] O. E. Jones, J. R. Holland, and W. B. Benedick, J. Appl. Phys. (to be published).
[4] R. W. Bancroft, D. Bancroft, B. L. Burton, T. Blechar, E. E. Houston, E. F. Gittings, and S. A. Landeen, J. Appl. Phys. **26**, 1472 (1955).
[5] D. H. Edwards, J. Sci. Instr. **35**, 346 (1958).

entire electrode face of the disk, (d) that an electric short-circuit exists between the two faces of the disk, and (e) that the strain is infinitesimal.

Assume the following about the physical properties of quartz: (f) that all stress amplitudes are steady and travel with the same wave velocity, (g) that the wave velocity is steady, (h) that the conductivity is zero, (i) that the dielectric permittivity does not change with finite shock stress and finite electric field, and (j) that the piezoelectric polarization is directly proportional to the x component of the stress by a coefficient f that is independent of time and stress for a given stress range.

Restricting the analysis to the one-dimensional case [assumptions (a) and (b)], the displacement current i due to the stress wave is

$$i=A\,dD/dt, \tag{1}$$

where A is the electroded area, D is the electric displacement (defined as $D=P+\epsilon E$), where P is the piezoelectric polarization, ϵ is the dielectric permittivity, and E is the electric field. We write the electric displacement as

$$\int_0^l D(x)dx=\int_0^l P(x)dx+\int_0^l \epsilon E(x)dx, \tag{2}$$

where l is the thickness of the disk, and the limits of integration chosen imply infinitesimal strain [assumption (e)]. Because of the short circuit [assumption (d)] and the constant permittivity [assumption (i)],

$$\int_0^l \epsilon E(x)dx=0. \tag{3}$$

For zero conductivity [assumption (h)], $\partial D/\partial x=0$ so that Eq. (2) now reduces to

$$D=\frac{1}{l}\int_0^l P(x)dx. \tag{4}$$

Further, $P(x)=f\sigma(x)$ [assumption (j)] and since the quartz is linearly elastic [assumptions (f) and (g)], $\sigma(x,t)=\sigma(x-U_s t)$, where U_s is the wave propagation velocity. The solution for the current from Eqs. (1) and (4) is then

$$i=A\frac{dD}{dt}=-\frac{fAU_s}{l}\int_0^l\frac{\partial\sigma(x)}{\partial x}dx=\frac{fAU_s}{l}[\sigma_0-\sigma_l], \tag{5}$$

where σ_0 is the x component of stress at the stress input electrode and σ_l is the x component of stress at the rear electrode. For times less than wave transit time

$$\sigma_0=(l/fAU_s)i, \quad 0<t<l/U_s. \tag{6}$$

Equation (6) predicts that the stress at the input electrode is directly proportional to the instantaneous current for times less than wave transit time. For times greater than wave transit time the stress difference between the two electrodes is directly proportional to the current.

EXPERIMENTAL TECHNIQUE

In order to study the physical properties of X-cut quartz and thereby determine the validity of assumptions (f)–(j), and to determine the behavior of various quartz disks insofar as assumptions (a)–(d) are concerned, an extensive experimental program has been accomplished. The experimental technique was designed to study the instantaneous relationship between current and stress. A number of improvements have been made since the technique was first reported.[6,7]

A well-defined shock stress is imparted to a specimen disk of X-cut quartz by the impact of a precisely aligned X-cut quartz disk used as a projectile facing, whose velocity at impact is accurately measured. This experimental configuration is shown schematically in Fig. 2. X-cut quartz exhibits a single wave structure for stress levels up to about 50 kbar[8,9]; consequently, we may compute the input stress to the specimen disk in the single wave region from the conservation of momentum relation

$$\sigma=\rho_0 U_s u_p, \tag{7}$$

where σ is the x component of stress imparted by the wave front, ρ_0 the density of the material ahead of the wave front, U_s the wave front propagation velocity, and u_p is the particle velocity imparted by the wave front. Because the impacting and impacted materials are the same, $u_p=\frac{1}{2}U_0$, where U_0 is the measured impact velocity.

If all assumptions are met unequivocally, Eq. (6) predicts the current, due to the constant particle velocity, to be constant for full wave transit time. The experimental method was to impart an accurately

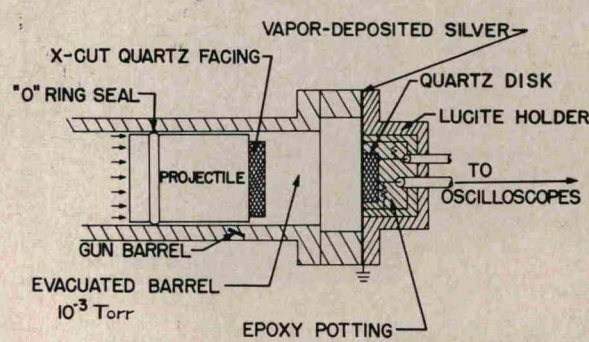

FIG. 2. Schematic of the experimental arrangement used to study the current from shock-loaded quartz disks.

[6] R. A. Graham, Rev. Sci. Instr. **32**, 1308 (1961).
[7] R. A. Graham, J. Appl. Phys. **32**, 555 (1961).
[8] J. Wackerle, J. Appl. Phys. **33**, 922 (1962).
[9] G. R. Fowles, Stanford Research Institute, Poulter Laboratories Technical Report 003-61 (1961).

measured particle velocity to various specimens of X-cut quartz disks and to record the current produced at stress levels from 3 kbar to about 50 kbar. Analysis of the current produced by the constant stress input permits the determination of certain of the physical properties of shock-loaded quartz, shows the effect of deviations from one-dimensional conditions, and serves as a quantitative calibration of the quartz disk for use as a gauge.

For a well-defined impact experiment, the angular misalignment of the impacting surface of the projectile facing and the impacted surface of the specimen disk (we call this "tilt") is sufficiently small so that the entire electrode of the disk is impacted in a time which is short compared to the stress wave transit time (typically 440 nsec). In the early experiments a propellant gun[10] with a $1\frac{5}{8}$-in. bore was used to accelerate the projectile to various velocities. A $2\frac{1}{2}$-in.-bore compressed-gas gun[11] has been used for the experiments performed most recently. Mean tilt values obtained were 5×10^{-4} rad for the gas gun and 1×10^{-3} rad for the propellant gun. The velocity of the projectile at impact is obtained by measuring the time interval for the projectile to move between two or sometimes three pairs of velocity stations in the immediate vicinity of the impact plane. The impact velocity thus obtained is known to $\pm0.5\%$.[12]

An important characteristic of the experiment is that the tilt of the impacting surfaces is indicated directly from the risetime of the current waveform. Furthermore, if partial loss of vacuum in the region ahead of the projectily occurs before impact, the resulting pressure build-up is clearly indicated by a slight precursor to the rapid rise in current due to the physical impact of the disks.

Nanosecond-type pulse circuitry was employed for all electrical measurements. The majority of the experiments were performed with signals imposed directly on the deflection plates of a Tektronix 517 oscilloscope. The resulting transmission line and oscilloscope risetime was measured to be 3 nsec. Some of the experiments were performed with Tektronix 545 oscilloscopes and Type L preamplifiers which gave a risetime of 12 nsec. The type of instrumentation used for a particular experiment is indicated in the tabulated results.

The characteristics of the experimental technique are such that the resulting data are remarkably self-contained, and the stress input conditions imposed on the specimen well-defined. All mechanical and electrical properties influence the data directly and the effect of qualifying conditions, such as tilt and pressure build-up, are clearly indicated on the records. This leads to a high degree of confidence in the physical circumstances under which the data were obtained. The experimental error in relating the values of particle velocity and current is estimated to be $\pm2\frac{1}{2}\%$.

THE GUARD-RING CONFIGURATION

A fully electroded disk with a small diameter-to-thickness ratio (d/l) shows considerable distortion to the idealized current pulse as is clearly shown in the typical $d/l=2$ record in Fig. 3. The current increases about 70% from the initial jump at $t=0$ to the final value at wave transit time, and the initial current is depressed about 15% below the one-dimensional case. Disks of various d/l ratios may be used for gauges on certain experiments, as will be shown later; but to study intrinsic physical properties and obtain undistorted gauge records, a one-dimensional configuration must be used. One-dimensional electric field and one-dimensional mechanical strain conditions are selectively obtained by using a quartz disk with a guard ring configuration. The inner portion of the disk is isolated electrically from the outer portion by separating the vapor-coated electrode into two regions as shown in Fig. 4. The potential on the two electrodes is kept approximately the same[13] by using resistive electrical loads whose resistances are in inverse proportion to the areas of the electrodes. By the proper choice of dimensions, the current observed from the inner region is obtained under one-dimensional conditions for the full transit time in the disk.

The electric field due to the piezoelectric effect in the stressed and unstressed portions of the disk is distorted by a number of mechanisms. At the outer edge of the disk the discontinuity in electric potential and dielectric permittivity causes electric field fringing in a manner similar to that encountered for parallel-plate capacitors under static conditions. The major differ-

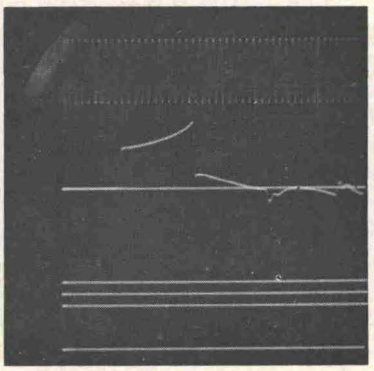

FIG. 3. Typical current–time record from small diameter-to-thickness disk. The disk was $\frac{1}{2}$ in. in diameter and $\frac{1}{4}$ in. in length. Shot H-56B time increases from left to right. 10-Mc/sec timing wave.

[10] R. A. Graham, G. E. Ingram, and W. D. Ingram, Sandia Corporation Research Report SC-4652 (RR) (November 1961).
[11] S. Thunborg, G. E. Ingram, and R. A. Graham, Rev. Sci. Instr. **35**, 11 (1964).
[12] G. E. Ingram, Rev. Sci. Instr. **36**, 458 (1965).

[13] Because the outer electrode region is not in a one-dimensional state, the current from the outer electrode suffers distortion similar to the bounded gauge distortion. Therefore, the potential on the two electrodes cannot be matched for all times. This does not have a significant effect on the field of the inner electrode region since the electric field corresponding to the potential difference between the electrodes is very small relative to the piezoelectric fields from the wavefront to the electrodes.

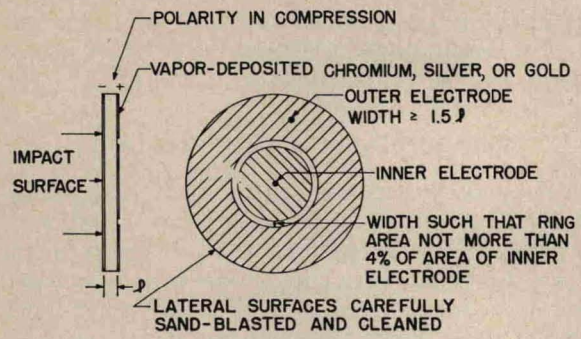

FIG. 4. Guard-ring configuration to obtain one-dimensional conditions.

ence in the dynamic case being considered here is that the traversing shock wave divides the disk into two regions of different field amplitudes whose lengths are time dependent. Hence, each region, the stressed and unstressed, has a different capacitive fringing factor and different time variation in the fringing factors. The guard ring eliminates this distortion by restricting the observation to the central region of the disk where there is negligible fringing.

As the wave moves along the disk in the axial direction, the boundary conditions require that shear and dilatational waves be formed immediately behind the wavefront at the lateral edge of the disk. These unloading waves then propagate laterally inward. Regions of the disk that experience these unloading waves from the lateral boundary are no longer in a state of one-dimensional strain. The central region of the disk will be in one-dimensional strain for the first wave transit time if the width of the outer electrode is such that an unloading wave does not reach the central region during first wave transit time.

However, since the medium is piezoelectric, the unloading waves change the polarization. To maintain constant electric displacement the electric field must also change. Field fringing would then be expected to occur from this unloading field and at any time the region of distorted field will be advancing radially inward in advance of the position of the unloading wave itself. Because of the anisotropy, no quantitative prediction was made of the width of outer ring required to take observations in one-dimensional field regions. However, we have empirically determined that the width of the outer ring must be no less than 1.5 times the thickness of the disk to completely eliminate this distortion during the first wave transit of a given stress amplitude.

The thin circular insulating ring cut through the electrode to form the inner and outer electrodes causes a local field distortion and an uncertainty as to the effective electrode area. In our experiments the width of the insulating ring was such that the area in the ring was from 2%–4% of the area of the inner electrode. Various ring widths in this range had no apparent effect on current from the disk. The small uncertainty in area due to the ring is calibrated into the guard-ring for disks constructed with rings whose width is in the range given above. Error is introduced if rings with large widths are used. The width of this ring cannot be easily reduced to less than 0.001–0.003 in. because a finite distance is required for dielectric strength between the two electrodes.

The features of a properly constructed guard-ring configuration are summarized in Fig. 4. Details of the proper construction of a guage, as given in Ref. 2, should be carefully followed.

GUARD–RING CURRENT COEFFICIENT

A typical guard-ring record is shown in Fig. 5 along with a definition of terms used in the data summary given in Table I. One should contrast this record with that shown in Fig. 3 to appreciate the distortion obtained with the fully electroded disk. However, even the current from the guard ring is observed to increase slightly as the wave propagates through the disk. It is shown in the Appendix that finite strain, an increase in dielectric permittivity with stress and electric field amplitude, and piezoelectric coupling will cause the current to increase linearly in time. The extent of the effect depends largely upon the stress amplitude. The current rise during transit time due to finite strain may be accurately calculated and is 4.8% at 20 kbar. The observed current rise of about 7% at 20 kbar shown in Table I (column 5) may be accounted for by the strain, an electromechanical coupling effect of 0.9%, and an increase of 0.6% in the dielectric permittivity of the stressed quartz.

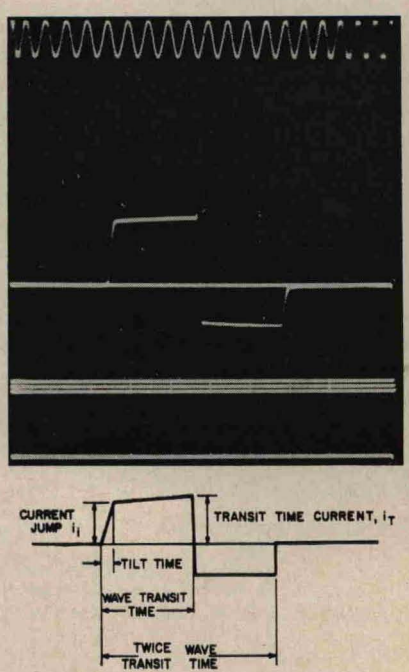

FIG. 5. Typical inner electrode guard-ring record and definition of terms. Time increases from left to right. 10-Mc/sec timing wave. Shot H-71.

TABLE I. Summary of one-dimensional guard-ring disk data.

Shot[a]	u_p[b]	σ[c]	k[d]	i_t/i_i[e]	Tilt[f] factor	Configuration[g]
H-82	0.01744	2.64	2.04	···	0.45	A
H-77	0.02952	4.47	2.06	1.03	0.34	A
H-75	0.04547	6.89	2.09	1.01	0.27	A
H-74	0.05105	7.74	2.11	1.03	0.10	A
H-84	0.06072	9.20	2.12	1.05	0.11	A
H-78	0.06087	9.23	2.13	1.05	0.17	A
H-76	0.06975	10.57	2.13	1.04	0.09	A
H-71	0.07827	11.86	2.13	1.05	0.11	A
H-70	0.09214	13.97	2.15	[h]	0.09	A
H-72	0.09275	14.06	2.14	[h]	0.02	A
H-67	0.1028	15.58	2.16	1.05	0.09	A
H-88	0.1119	16.96	2.18	1.08	0.09	A
H-62	0.1137	17.23	2.18	1.06	0.13	A
H-89	0.1167	17.69	2.18	1.08	0.06	A
H-90	0.1252	18.98	2.23	1.08	0.08	A
H-61	0.1292	19.58	2.27	1.08	0.14	A
H-64	0.1337	20.26	2.27	1.08	0.09	A
P-231	0.0281	4.26	2.04[k]	[j]	0.64	C
P-241	0.0398	6.03	2.02	[j]	0.44	C
P-242	0.0465	7.05	2.10	1.03	0.25	C
P-243	0.0552	8.37	2.11[l]	1.05	0.33	D
P-227	0.0638	9.67	2.14[l]	1.03	0.20	C
P-251	0.0700	10.61	2.13	1.03	0.11	D
P-225	0.0941	14.26	2.17	1.05	0.20	C
P-228	0.1080	16.37	2.15	1.06	0.21	C
P-226	0.1197	18.14	2.16	1.05	0.36	C
P-234	0.1252	18.98	2.21	1.05	0.45	E
P-235	0.1270	19.25	2.25	1.05	0.43	F
P-237	0.1345	20.39	2.23	1.07	0.35	G
P-258	0.1440	21.83	2.24	1.10	0.16	C
P-229	0.1547	23.45	2.38	1.08	0.15	C
P-224	0.1555	23.57	2.26	1.07	0.12	H
P-259	0.1661	25.18[m]	2.29	1.08	0.10	C
P-230	0.2201	33.67[m]	2.41	[n]	0.23	C
P-261	0.2644	41.04[m]	2.48	1.21[n]	0.12	C
P-260	0.2672	41.51[m]	2.38	[o]	0.10	C
P-233	0.2886	45.01[m]	2.38	[o]	0.15	C
P-256	0.3118	48.82[m]	2.43	[n]	0.07	D

[a] H prefix indicates experiments on compressed-gas gun. P prefix indicates experiments on propellant gun. H experiments recorded on direct deflection 517 oscilloscopes with risetime 3 nsec. P experiments recorded on 545 oscilloscopes, L preamplifier, risetime 12 nsec.

[b] u_p is particle velocity at impact surface. Computed as one-half the measured impact velocity. Units are mm-μsec^{-1}.

[c] σ is impact stress ($\rho U_s u_p$), computed from particle velocity using $\rho=2.650$ g-cm^{-3} and $U_s=5.72$ mm-μsec^{-1}, except as noted. Units are kbars.

[d] k is the current coefficient computed from the expression $k=(l/Ac_{11})(i_t/u_p)$. The area is computed from the measured diameter of the inner electrode. Values of A and l are thus known to an accuracy of $\pm 0.1\%$. Bechmann's value $c_{11}=86.74\times10^{10}$ dyn-cm^{-2} is used for k computation from zero to 25 kbar and verified experimentally by the U_s readings. For stress greater than 25 kbar, c_{11} is computed from the expression $c_{11}=\rho U_s^2$, where $\rho=2.65$ g-cm^{-3} and U_s is the least-squares fit to the velocity measurements. Units are 10^{-8} C-cm^{-2}-kbar^{-1}.

[e] i_i is current jump. i_t is current at transit time. i_t/i_i is a measure of the increase in current during wave-transit time.

[f] The tilt factor is the ratio of the measured time to impact the electroded area to the wave-transit time.

[g]
A	1½ in. o.d.	0.100 in. thick	0.6-in.-diam inner electrode
C	1½ in. o.d.	0.100 in. thick	0.5
D	1½ in. o.d.	0.125 in. thick	0.5
E	1½ in. o.d.	0.100 in. thick	0.63
F	1½ in. o.d.	0.100 in. thick	0.38
G	1½ in. o.d.	0.100 in. thick	1.0
H	1½ in. o.d.	0.150 in. thick	0.5

[h] Slight pressure increase prior to impact.

[j] Cannot measure current rise accurately due to large tilt values.

[k] k computed from integrated current.

[l] $-X$ orientation—no conductivity observed.

[m] Stress computed from $U_s=5.57+1.08u_p$ mm-μsec^{-1} which is the linear east-squares fit to the data above 25 kbar.

[n] Current–time observed is nonlinear.

[o] Current discontinuities before completed wave transit.

The observed current–stress relationship is expressed by defining a current coefficient

$$k=i_t l/\sigma A U_s=i_t l/u_p A c_{11}, \tag{8}$$

where i_i is the measured current jump and $c_{11}=\rho U_s^2$. The low-signal constant-field elastic-stiffness constant c_{11}^E given by Bechmann[14] was used in the computation of k for stress less than 25 kbar. For stress greater than 25 kbar an elastic stiffness coefficient was computed from the observed wave velocity given below. The experimental values of the current coefficient are k 2.04×10^{-8} C-cm^{-2}-kbar^{-1} for stress from zero to 6 kbar and $k=2.15\times10^{-8}$ C-cm^{-2}-kbar^{-1} from 9–18 kbar. All observed experimental points are within $\pm1.5\%$ of the mean values quoted. Above 18 kbar the coefficient is continuously variable. From these data we conclude that the limit of low-signal piezoelectric behavior for shock-loaded X-cut quartz is 6 kbar. This conclusion is further strengthened by the fully electroded data shown below.

In the low stress limit we obtain a direct measure of the piezoelectric stress constant e_{11}. From Eqs. (6)–(8), and an area correction for the effect of the ring, we find that

$$e_{11}=kc_{11}A/A_e, \tag{9}$$

where A is the area of the inner electrode and A_e is the effective area of the inner electrode. This is taken as A plus one-half the area of the insulating ring. Our value is compared to recent determinations by other authors[14,15] in Table II. It should be emphasized that

TABLE II. Observed piezoelectric stress constant e_{11}.

Present work	0.174 C-m^{-2}
Bechmann[14]	0.171
Koga *et al.*[15]	0.175

in the low stress limit, this technique gives e_{11} directly and that the value obtained is not dependent upon the value chosen for the elastic stiffness. It should also be emphasized that the current coefficient was computed from the area of the inner electrode; therefore, the inner electrode area, not A_e, should be employed in Eq. (6) when using the quartz disk as a gauge.

From the transit time indicated on the current–time record we obtain a direct measure of the propagation velocity in the single wave region. The least-squares fit to the U_s vs u_p data is

$$0<\sigma<25 \text{ kbar} \quad U_s=5.740(s=0.04)-0.14u_p(s=0.24) \text{ mm-}\mu\text{sec}^{-1}$$
(23 observations),

$$25<\sigma<50 \text{ kbar} \quad U_s=5.57(s=0.10)+1.08u_p(s=0.44) \text{ mm-}\mu\text{sec}^{-1}$$
(12 observations),

where s is the standard deviation.

[14] R. Bechmann, Phys. Rev. **110**, 1060 (1958).

[15] I. Koga, M. Aruga, and Y. Yoshinaka, Phys. Rev. **109**, 1467 (1958).

The fit from atmospheric pressure to 25 kbar shows that the wave velocity changes less than $\frac{1}{2}\%$ with a mean value of 5.728 mm/μsec. Hence, the current coefficient determination which relates current to stress is accomplished with an estimated accuracy of $\pm 3\%$ in the stress range to 25 kbar.

The standard deviations of the coefficients for the wave velocity least-squares fit for stress amplitude greater than 25 kbar are large; however, a comparison of computed values from our least-squares fit with those of Wackerle[8] (Table III) shows excellent agreement.

TABLE III. Comparison of least-squares fit to wave velocity determination above 25 kbar.

u_p	U_s Wackerle	U_s Present work
0.1661 mm-μsec^{-1}	5.76 mm-μsec^{-1}	5.75 mm-μsec^{-1}
0.2201	5.81	5.81
0.2644	5.85	5.86
0.2672	5.85	5.86
0.2886	5.87	5.88
0.3318	5.89	5.91

For the stress region above about 30 kbar the current from the disk is generally less predictable and shows nonlinear current–time effects apparently due to dielectric permittivity changes and conduction. These effects limit accurate use of the guard-ring disk as a gauge to the measurement of stress jumps.

In agreement with previous observations on bounded disks,[16] internal conduction is observed for quartz in the $-X$ orientation in the guard-ring gauge configuration. Conduction does not occur for the $+X$ orientation guard-ring disk for the stress range up to about 30 kbar. The $+X$ orientation is obtained by orienting the disk such that a compressive stress wave propagates from the $-X$ electrode to the $+X$ electrode. The polarity of the electroded faces of the disk is determined with the gauge in compression. For a quantitative analysis of the effect of finite resistivity on piezoelectric current the reader is referred to Wittekindt.

FULLY ELECTRODED DISKS

For many experiments a fully electroded disk can be used as a gauge if the resulting distortion of the current waveforms is known; for example, the results of Jones *et al.*[1] were obtained with the fully electroded gauge. The gauge is constructed from an X-cut quartz disk in a manner similar to the guard-ring gauge, except that the guard ring is not formed and the $+X$ electrode is placed in direct contact with an aluminum disk that has the same diameter as the quartz. Electrical connection is made to the aluminum disk.

Typical records obtained with a step input of stress into various fully electroded disks are shown in Fig. 6. The pronounced distortion in current compared to the current from the guard-ring configuration is apparent. The extent of the distortion depends upon the particular d/l ratio of the disk and, as expected, is more pronounced for the gauges with a smaller d/l ratio.

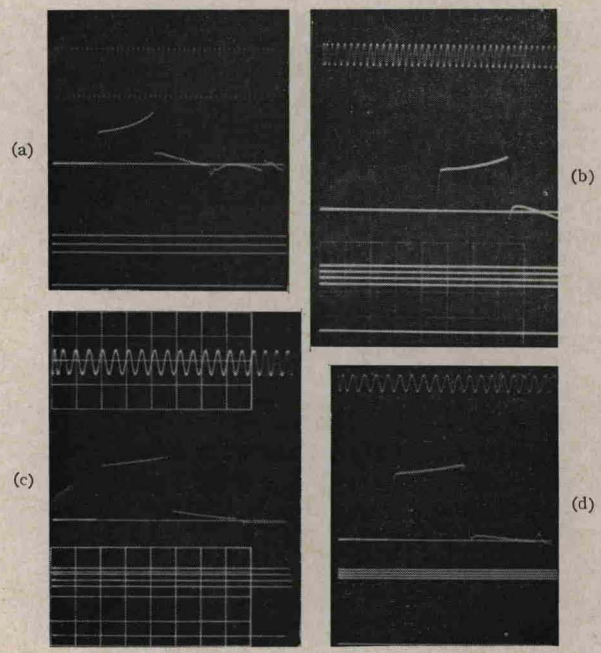

FIG. 6. Typical current–time records from various diameter-to-thickness ratio disks. Time increases from left to right. (a) $d/l=2$, Shot H-56B, 10-Mc/sec timing wave. (b) $d/l=4$, shot 97C, 5-Mc/sec timing wave. (c) $d/l=10$, shot 104B, 10-Mc/sec timing wave. (d) $d/l=16.7$, shot 79A, 5-Mc/sec timing wave.

If tilt is negligible the current jump at impact time should not be affected by unloading waves from the lateral boundary. However, distortion to this current jump can be caused by electrostatic field distortion. Early in the propagation time the stressed region is very thin with the result that the field lines in the stressed portion are not severely distorted. The unstressed region, however, is relatively thick and, depending upon the d/l ratio of the disk, considerable distortion to the field lines will be present. The effect of the field fringing on the current jump is analyzed in the Appendix by considering the relative field fringing between the stressed and unstressed regions of the disk. This relative field fringing has the same effect as a difference in permittivity between the two regions causing the current jump to be depressed below that predicted for the one-dimensional case. As the wavefront progresses through the disk the relative field distortion between the stressed and unstressed regions of the disk changes until, finally, at wave-transit time the unstressed region is relatively undistorted and the stressed region shows distortion. Late in the first-wave transit we would also expect the piezoelectric response due to the unloading waves from the lateral boundaries

[16] R. A. Graham, J. Appl. Phys. 33, 1755 (1962).
[17] R. H. Wittekindt, Harry Diamond Laboratory Report No. TR-922 (May 1961).

TABLE IV. Summary of full electrode disk data.[a]

Shot	u_p	σ	k	i_t/i_i	Tilt factor	Configuration	
H-34	0.1233	18.69	2.18	1.06	0.52	$1\frac{1}{4}\times0.050$ in.	$d/l=25$
H-33	0.1284	19.46	2.15	1.08	0.58		
H-79B	0.1242	18.83	2.21	1.05	0.50	$\frac{1}{2}\times0.025$ in.	
80B	0.1413	21.42	2.18	1.05	0.37		$d/l=20$
81B	0.2109	32.4	2.30	1.12	0.41		
H-79A	0.1242	18.83	2.11	1.14	0.14	$1\frac{1}{4}\times0.075$ in.	
80A	0.1413	21.42	2.16	1.15	0.16		$d/l=16.7$
99	0.1602	24.28	2.10	1.18	0.18		
81A	0.2109	32.4	2.26	1.17	0.27		
H-104B	0.07043	10.68	1.98	1.16	0.11	$1\frac{1}{4}\times0.125$ in.	
116B	0.1008	15.28	2.05	(b)	0.13		$d/l=10$
107B	0.1476	22.37	2.08	1.26	0.04		
109	0.2193	33.8	2.26	1.19	0.35		
H- 97B	0.09552	14.48	1.99	1.35	0.05	$1\frac{1}{4}\times0.25$ in.	
98B	0.1563	23.69	2.07	1.46	0.04		
100B	0.1893	28.9	2.04	1.46	0.07		$d/l=5$
101B	0.2393	37.0	1.89	1.78	0.11		
102B	0.3129	49.0	2.11	1.79	0.05		
H-104A	0.07043	10.68	1.95	1.17	0.43	$\frac{1}{2}\times0.1$ in.	
116A	0.1008	15.28	1.96	(b)	0.05		
106	0.1060	16.07	2.02	1.20	0.37		$d/l=5$
107A	0.1476	22.37	2.11	1.36	0.11		
109A	0.2193	33.8	2.16	1.43	0.17		
110	0.2886	45.0	2.22	1.31	0.44		
H-97C	0.09552	14.48	2.07	1.33	0.06	$\frac{1}{2}\times0.125$ in.	$d/l=4$
98C	0.1563	23.69	2.03	1.47	0.06		
H-49	0.01948	2.95	1.75	(b)	0.27	$\frac{1}{2}\times0.25$ in.	
55	0.01956	2.96	1.70	1.83	0.08		
39	0.02569	3.89	1.70	1.71	0.09		
38	0.03474	5.27	1.73	1.73	0.27		
56A	0.06650	10.08	1.94	1.50	0.18		$d/l=2$
B	0.06650	10.08	1.87	1.61	0.06		
C	0.06650	10.08	1.95	1.45	0.10		
97A	0.09552	14.48	1.85	1.87	0.04		
98A	0.1563	23.69	1.75	2.13	0.03		

[a] Definitions of terms and units are the same as those used in Table I.
[b] i_t not recorded due to partial experimental failure.

to cause further distortions to the current waveform.

The data from the investigation of the fully electroded disk are shown in Table IV. A surprising result is that the current coefficient for the fully electroded disk is essentially constant for the stress range of 9 to about 25 kbar.

Table V summarizes the current coefficients for the various configurations. For a given stress, the k values are definitely lower for the smaller d/l ratio gauges. For gauges with $d/l\geq20$ the k values obtained are the same within experimental error as those obtained for the guard ring. For large d/l-ratio disks we would expect the current waveform to approach the one-dimensional guard-ring current waveform since both field fringing and unloading wave effects become negligible during the first-wave transit time.

The current–time record of a typical fully electroded disk shows a nonlinear current rise in time after the initial current jump. However, disks with $d/l\geq10$ show a linear current rise. For the $d/l=5$ disk, the current rise is linear for about one-half wave-transit time and then becomes nonlinear. For disks with $d/l\leq4$, the current is nonlinear in time for essentially the entire wave-transit time.

TABLE V. Current coefficient for various fully electroded disks. Mean values for stress between 9–25 kbar.

Diameter thickness ratio	k_{mean}
2	1.90
4	2.05
5	2.05
5	2.05
10	2.04
16.7	2.12
20	2.20
25	2.17

The experiments on $d/l=2$ disks confirm that there is a stress region below 6 kbar for which the current coefficient does not change. Further, the difference observed in k between the $d/l=5$ and $d/l=16.7$ disks agrees with the determination of Jones *et al.*[1]

For an input stress greater than 25 kbar, considerable distortion to the current–time waveform occurs due to conduction. The distortion is greater for the more bounded disks, indicating that the conduction is more pronounced in the regions of the gauge affected by the unloading waves. For this reason, at stress amplitudes greater than 25 kbar, the bounded disk is an accurate gauge only for the current jump.

Since the current jump is directly affected by the capacitive field fringing of the disk, the values of k quoted here for the small d/l disks are strictly applicable only for the electrode configuration used here, which is a ground plane of essentially infinite extent and a positive electrode the same size as the disk. A potting compound of radically different dielectric permittivity could conceivably alter the field fringing behavior.

CONCLUSION

Despite the fact that local strain and resulting polarization are coupled to each other with the speed of light in a piezoelectric medium, time-dependent effects are possible through variable wave velocity, strain relaxation, dielectric permittivity relaxation, or conduction. Our analysis of the data indicates that for stress less than about 25 kbar and for disks in the $+X$ orientation it is possible to describe all aspects of our data to time-independent physical properties. The most rapid stress application possible with existing gun and explosive-loading techniques within the useful stress range of the gauge is 10^{-8} sec over a $\frac{1}{2}$-in.-diam inner electrode. However, the rate of stress application to a given point on the surface is certainly higher. For the range of stress rates achieved in shock experiments and for stress values below about 25 kbar we conclude that there are no detectable rate effects. Our results define the appropriate physical properties of X-cut

quartz with sufficient accuracy so that the current from quartz disks may be used for detecting stress–time profiles with a stress-amplitude accuracy comparable to other shock detection techniques and with a superior time resolution.

ACKNOWLEDGMENTS

The authors are indebted to numerous colleagues at Sandia Laboratory for helpful and stimulating discussions; to W. D. Ingram for specimen preparation and mechanical assistance; and, particularly, to G. E. Ingram who designed the electronic circuitry and developed methods to obtain the precise alignments required.

APPENDIX

An analysis is given for the effects of finite strain, dielectric permittivity change, parallel-plate capacitive field fringing and piezoelectric coupling on the current generated in an X-cut quartz disk subjected to a step function of stress.

General Expressions

For the particular case of a step function of stress assumptions (a)–(j) we may derive equations for electric field and current. At any time during the first wave transit the disk is divided into two regions: the unstressed region (denoted by subscript 1 hereafter) and the stressed region (denoted by subscript 2 hereafter).

For zero conductivity,

$$D_1=D_2, \tag{A1}$$

where D is the electric displacement.

Since an electric short circuit exists between the two electrodes,

$$E_2l_2=-E_1l_1. \tag{A2}$$

We know that

$$l_2=U_st, \quad \text{and} \quad l_1=l-U_st. \tag{A3}$$

Solving for E_2 in terms of E_1 from Eq. (A2) and substituting this into Eq. (A1), we find that

$$E_1=PU_st/\epsilon l, \tag{A4}$$

and

$$E_2=P(1-U_st/l)/\epsilon. \tag{A5}$$

The magnitude of the field in the stressed region of the disk at a stress of 20 kbar and at $t=0+$ is 1.13×10^5 V-cm^{-1}. The presence of these large fields requires that the lateral surface of the gauge be exceptionally clean and carefully potted.

From Eqs. (A1) and (1) we find that the current is

$$i=PAU_s/l, \quad 0<t<l/U_s, \tag{A6}$$

in agreement with Eq. (6).

Finite Strain

For the case of finite strain s,

$$l_2=NU_st, \quad \text{and} \quad l_1=l-U_st,$$

where

$$N=1-s.$$

Again we obtain the current by solving for E_2 in terms of E_1 and substituting this into Eq. (A1) and (1). The solution is

$$i=PAU_slN[U_st(N-1)+l]^{-2}. \tag{A7}$$

Neglecting $(N-1)^2$ terms, we find that

$$i_t/i_i=(2N-1)^{-1}. \tag{A8}$$

From the known elastic stiffness we find the value of this ratio to be 1.048 at 20 kbar. For the strain involved in the usual gauge experiment Eq. (A7) predicts a linear increase in current with the time to a close approximation.

Dielectric Permittivity Change

If the dielectric permittivity in the stressed region has a value different from the unstressed region, we examine the effect on the current by solving for the current in the same manner as done previously except to allow $\epsilon_1\neq\epsilon_2$. The solution for current is

$$i=PAU_sl\epsilon_2/\epsilon_1[U_st+\epsilon_2(l-U_st)]^2. \tag{A9}$$

The current ratio is

$$i_t/i_i=(\epsilon_2/\epsilon_1)^2. \tag{A10}$$

For small differences between ϵ_2 and ϵ_1 the current increases linearly in time to a close approximation.

Time-Dependent Parallel-Plate Capacitive Field Fringing

To analyze the effect of the field fringing for the fields between the stress wave front and the electrodes it is convenient to express the current in terms of the time varying series capacitance of the stressed and unstressed regions. First consider the one-dimensional field case. Because of the electric short-circuit condition

$$q_1/C_1=q_2/C_2, \tag{A11}$$

where q is the charge on the capacitor and C, the time-dependent capacitance for one-dimensional fields between the wavefront and the electrodes.

Further,

$$q_2=PA-q_1. \tag{A12}$$

We can solve for q_1 from Eq. (A12) and (A11). Differentiating the charge with respect to time gives

$$i=dq/dt=PA[C_2dC_1/dt-C_1dC_2/dt][C_1+C_2]^{-2}. \tag{A13}$$

If we substitute the expressions for the time-depend-

ent thickness for the stressed and unstressed regions, Eq. (A13) reduces to Eq. (6).

For the case of field fringing the capacitance of each region differs from the one-dimensional capacitance.

Let

$$\lambda = C_\lambda / C,$$

where C_λ is the capacitance between the wavefront and the electrodes including field fringing effects, C is the capacitance for one-dimensional field, and λ is the fringing factor.

In the manner of the one-dimensional derivation, we derive the current, including field fringing effects. The current is

$$i_\lambda = PA\{\lambda_1\lambda_2[C_2(dC_1/dt) - C_1(dC_2/dt)] + C_2C_1(\lambda_2 d\lambda_1/dt - \lambda_1 d\lambda_2/dt)\}(\lambda_2 C_2 + \lambda_1 C_1)^{-2}. \quad \text{(A14)}$$

In order to numerically evaluate the effect of fringing on the current, measurements of the capacitance of various diameter-to-thickness disks were made. From these data we determined approximate values for λ and $d\lambda/dt$. Our calculations showed that the effect of this type of field fringing was to depress the current jump below the value for the one-dimensional case with the extent of the effect depending upon the d/l ratio for the disk. This result is in agreement with the experimental observations on the full electrode gauges.

Electromechanical Coupling

The elastic stiffness of the quartz changes slightly with time due to electromechanical coupling. We evaluate this effect below.

The piezoelectric equation of state for one-dimensional strain along the x axis is

$$\sigma = c_{11}^E s - e_{11} E. \quad \text{(A15)}$$

Substituting the field from Eq. (A5) into Eq. (A15), we find that

$$\sigma = c_{11}^E s + e_{11} P(1 - U_s t/l)/\epsilon = s[c_{11}^E + e_{11}^2(1 - U_s t/l)/\epsilon]. \quad \text{(A16)}$$

From the one-dimensional wave equation we know that

$$\rho U_s^2 = \partial\sigma/\partial s; \quad \text{(A17)}$$

hence

$$\rho U_s^2 = c_{11}' = c_{11}^E[1 + e_{11}^2(1 - U_s t/l)/c_{11}^E\epsilon]. \quad \text{(A18)}$$

When $t=0$ we find that

$$c_{11}' = c_{11}^E[1 + e_{11}^2/c_{11}^E\epsilon] = c_{11}^D,$$

and when $t = l/U_s$

$$c_{11}' = c_{11}^E = c.$$

Bechmann finds $c_{11}^E = 86.74\times10^{10}$ dyn-cm^{-2} and $c_{11}^D = 87.49\times10^{10}$ dyn-cm^{-2}. This analysis demonstrates that the elastic stiffness is slightly time dependent due to electromechanical coupling. A more extensive analysis by Baerwald[18] indicates that the electromechanical coupling will cause the current to increase by a factor $e^2/c\epsilon$ during wave transit time.

---

[18] H. G. Baerwald, Sandia Laboratory (private communication).

Issued by
Technical Information Division III
Sandia Corporation
Albuquerque, New Mexico